Pergamon

PII: S0191-8141(98)00046-7

Journal of Structural Geology, Vol. 20, No. 8, pp. 1121 to 1137, 1998
© 1998 Elsevier Science Ltd
All rights reserved. Printed in Great Britain
0191-8141/98 $19.00 + 0.00

Monoclinic model shear zones

C. W. PASSCHIER

Department of Geosciences, University of Mainz, 55099 Mainz, Germany, E-mail: jsg@mail.unimainz.de

(*Received* 23 *April* 1997; *accepted in revised form* 21 *April* 1998)

Abstract—Although many ductile shear zones are supposed to have developed by approximately simple shear flow, some must have formed under different conditions. A few types of such 'non-simple shear zones' have been proposed in the literature such as transpression-, transtension- and stretching-shear zones. This paper presents a full three-dimensional kinematic model of shear zones with monoclinic flow geometry. Monoclinic shear zone types can be classified according to flow parameters, and according to the geometry and orientation of accumulating finite strain. Modelling of finite strain accumulation shows that a number of unusual and potentially problematic structural features may develop in monoclinic shear zones. These include stretching lineations normal to the displacement direction; foliations normal to the shear zone boundary; switching of the position of principal finite strain axes X, Y and Z during progressive deformation; and strain gradients along shear zones that may give rise to obliqueness of fabric elements of the same age in adjacent rock volumes. © 1998 Elsevier Science Ltd. All rights reserved

INTRODUCTION

The literature on ductile shear zones is mostly concerned with the geometry of zones from the upper crust, formed under greenschist to lower-amphibolite facies conditions. Many of these shear zones apparently formed by simple shear progressive deformation in planar zones with a rigid wall rock (Fig. 1a). Development of fabrics in such 'simple shear zones' is relatively well understood (cf. Ramsay, 1980; Ramsay and Huber, 1983). However, progressive deformation histories other than simple shear (cf. Simpson and DePaor, 1993) may operate in ductile shear zones with deforming wall rocks, especially at high-grade metamorphic conditions; the most commonly cited types in the literature are transpression-, transtension-, stretching- and shortening-shear zones (Fig. 1; Harland, 1971; Sanderson and Marchini, 1984; Kligfield and Crespi, 1984; Means, 1989; Paterson and Wainger, 1991; Fossen and Tikoff, 1993; Krantz, 1995; Jones and Tanner, 1995; Jiang and White, 1995; Tikoff and Greene, 1997; Jones *et al.*, 1997). Most of these shear zone models are based upon specific flow types with a monoclinic symmetry in the absence of volume change. In this paper, I wish to explore all possible monoclinic flow types to see what finite strain fabrics could result, and how this could affect fabrics in planar shear zones that operate by monoclinic flow types. Although this is largely a theoretical exercise, the results may be applicable to segments of shear zones where flow and deformation were approximately homogeneous (Figs 1 & 2).

MONOCLINIC FLOW

In any type of homogenous flow, three orthogonal axes can be defined that are known as the instantaneous stretching axes (ISA; Passchier, 1991); two of these axes represent directions of maximum and minimum stretching rate of material lines (Lister and Williams, 1983; Passchier, 1988). In this paper, the ISA are defined as vectors $\mathbf{a_I}$, $\mathbf{a_{II}}$ and $\mathbf{a_{III}}$ where a_{I}, a_{II} and a_{III} are the magnitudes of stretching rates of material lines instantaneously parallel to ISA (Fig. 2). Throughout this paper, the ISA are described as fixed in orientation in an external reference frame, but shear zone boundaries and finite strain axes may be rotating in this reference frame (Fig. 2). The value of $a_{\mathrm{II}} > a_{\mathrm{III}}$ by definition to avoid duplication of mirror-image flow types. In an external reference frame in which ISA are fixed, material lines that are instantaneously parallel to ISA can either remain parallel to them (coaxial flow) or rotate with respect to ISA and the external reference axes (non-coaxial flow). The rotational component of flow can be described by a vorticity vector $\mathbf{w}$ which need not be parallel to any ISA. In this paper, flow in model shear zones has a monoclinic symmetry with $\mathbf{w}$ parallel to $\mathbf{a_I}$ (Fig. 2); w is the sum of the angular velocity of material lines instantaneously parallel to $\mathbf{a_{II}}$ and $\mathbf{a_{III}}$ (Passchier, 1997).

Any type of monoclinic flow can be fully defined by the four numbers a_{I}, a_{II}, a_{III} and w. Alternatively, *three* normalised, dimensionless numbers W_{n}, A_{n} and T_{n} can be used to describe the *geometry* of monoclinic flow (Passchier, 1997). This has the advantage that flow types can be compared without reference to absolute particle velocities or stretching rates. The numbers are defined as the *sectional kinematic vorticity number*

$$W_{\mathrm{n}} = \frac{w}{2\dot{s}} = \frac{w}{a_{\mathrm{II}} - a_{\mathrm{III}}}, \tag{1}$$

the *sectional kinematic dilatancy number*

$$A_{\mathrm{n}} = \frac{a_{\mathrm{II}} + a_{\mathrm{III}}}{2\dot{s}} = \frac{a_{\mathrm{II}} + a_{\mathrm{III}}}{a_{\mathrm{II}} - a_{\mathrm{III}}} \tag{2}$$

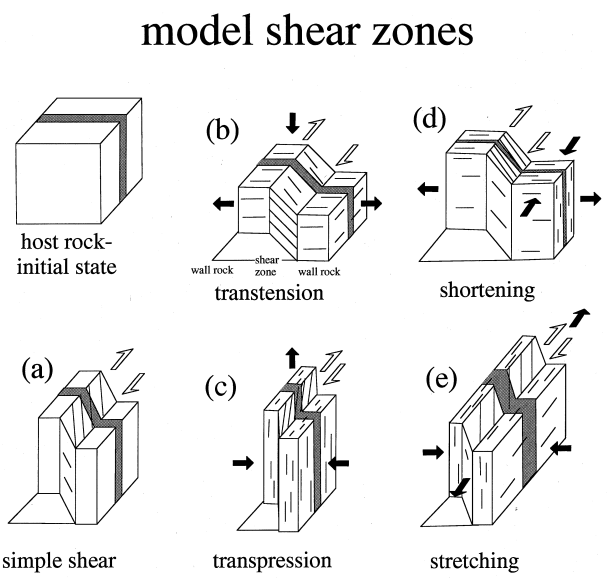

Fig. 1. Different types of three-dimensional model shear zones as described in the literature. Further explanation in the text.

and the *sectional kinematic extrusion number*

$$T_n = \frac{a_I}{2\dot{s}} = \frac{a_I}{a_{II} - a_{III}} \quad (3)$$

$\dot{s}$ is the mean stretching rate:

$$\dot{s} = \frac{a_{II} - a_{III}}{2}. \quad (4)$$

The sum of T_n and A_n is V_n, the *kinematic volume change number*

$$V_n = T_n + A_n = \frac{a_I + a_{II} + a_{III}}{2\dot{s}} = \frac{a_I + a_{II} + a_{III}}{a_{II} - a_{III}} \quad (5)$$

In monoclinic flow with ISA fixed in an external reference frame, up to three axes can be found where material lines do not rotate with respect to this reference frame; the flow eigenvectors **d**, **e** and **f** (Fig. 2; Passchier, 1997).The eigenvectors **d** and **e** are symmetrically arranged with respect to the ISA $\mathbf{a_{II}}$ and $\mathbf{a_{III}}$, but not orthogonal except in coaxial flow where they coincide with the ISA $\mathbf{a_{II}}$ and $\mathbf{a_{III}}$ (Fig. 2). The eigenvector **f** is unusual in that it is identical to one of the ISA, $\mathbf{a_I}$. The eigenvectors **d, e** and **f**, also known as 'flow apophyses' (Ramberg, 1975), play an important role in fabric accumulation and the classification of shear zones, as outlined below. Since $a_{II} > a_{III}$ by definition, $e \geq d$ in any monoclinic flow type (Passchier, 1991). In monoclinic flow as presented in this paper, either **e** or **f** can be an attractor of material lines (ML-attractor; Passchier, 1997).

CLASSIFICATION OF MODEL SHEAR ZONES BY FLOW TYPE

In this paper, flow in model shear zones is homogeneous and the boundary to the wall rock is a coherent interface. Even though flow in the zone is defined to have monoclinic symmetry, described by W_n, A_n and T_n, the shear zone itself will only have a monoclinic *geometry* if the shear zone boundary is parallel to the $\mathbf{a_I}$–**f**–**w** axis (Fig. 2). If the shear zone boundary should remain *irrotational* in the external reference frame and with respect to ISA of flow in the zone, it must be parallel to either **d** or **e** as well, and flow geometry should not change with time. Thus, two types of 'irrotational' monoclinic model shear zones can be defined, with boundaries parallel to **f** and **d** (**df**-shear zones), or to **f** and **e** (**ef**-shear zones) (Fig. 3a & b). Most published shear zone models classify as **ef** or **df**-shear zones (e.g. Ingles, 1983; Sanderson and Marchini, 1984; Weijermars, 1991; Fossen and Tikoff, 1993; Tikoff and Fossen, 1993; Krantz, 1995).

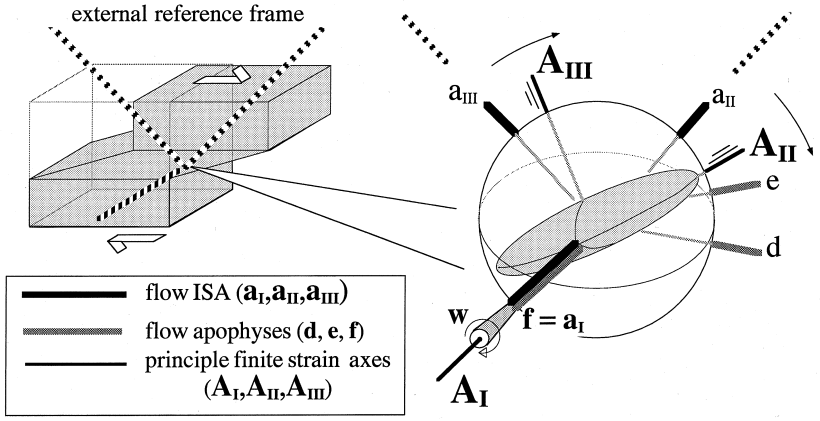

Fig. 2. Model shear zone and inset showing the orientation of flow and strain axes mentioned in the text. $\mathbf{a_I}$, $\mathbf{a_{II}}$, $\mathbf{a_{III}}$—instantaneous stretching axes. These are permanently fixed parallel to coordinate axes of an external reference frame as indicated. **w**—vorticity vector. **d**, **e** and **f**—flow apophyses (eigenvectors). The orientation of principal finite strain axes is labelled $\mathbf{A_I}$, $\mathbf{A_{II}}$ and $\mathbf{A_{III}}$. $\mathbf{A_{II}}$ and $\mathbf{A_{III}}$ lie in one plane with $\mathbf{a_{II}}$, $\mathbf{a_{III}}$, **d** and **e**. Since flow in the zone has a monoclinic symmetry, $\mathbf{a_I}$, **f**, **w** and $\mathbf{A_I}$ are all parallel. **f** and $\mathbf{a_I}$ are identical. In most flow types, $\mathbf{A_{II}}$ and $\mathbf{A_{III}}$ rotate in the external reference frame.

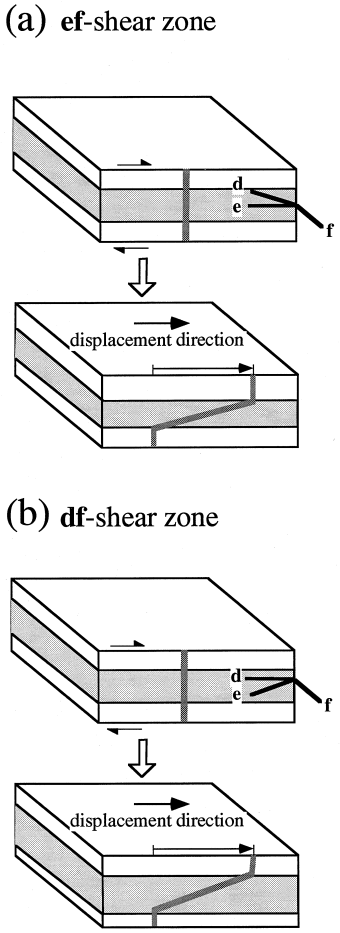

Fig. 3. Diagrams showing initial (top) and final (bottom) stages in the development of **ef**- and **df**-shear zones. The grey line on the front of the diagrams is a marker line used to illustrate the concept of displacement direction. **f**, **d** and **e** are flow apophyses in the shear zone. (a) **ef**-shear zone, where the shear zone boundary is parallel to **f** and **e**. (b) **df**-shear zone, where the shear zone boundary is parallel to **f** and **d**.

In simple shear zones, the relative displacement direction of the rigid wall rocks parallel to shear zone boundaries can be referred to as the 'shear direction' or 'direction of tectonic transport'. In model shear zones with deforming wall rocks described in this paper the 'displacement direction' is defined as a vector parallel the shear zone boundaries that traces the offset of a marker line drawn normal to the boundaries at the onset of deformation (Fig. 3).

Classification of **df**- *and* **ef**-*shear zones*

df- and **ef**-shear zones can be classified according the geometry of flow in the zone as expressed by the parameters W_n, T_n, A_n and V_n. Figure 4(a) is an example of a diagram that represents W_n–A_n–T_n space, and in which each monoclinic flow type can be presented by a point (Passchier, 1997). Flow types with the same relative volume change rate (V_n) plot on planes dipping to the right (Fig. 4b & c). Further subdivision is possible by considering the properties of flow apophyses.

Flow apophyses can be divided into three types: those along which material lines instantaneously extend, shorten, or remain constant in length (Fig. 5a, inset). Monoclinic isochoric flow ($V_n = 0$) in **df**- and **ef**-shear zones can be classified into 17 types according to combinations of the three types of apophyses, as illustrated in Fig. 5(a) on a planar section through W_n–A_n–T_n-space for $V_n = 0$ (the right-dipping plane in Fig. 4a). In contrast to V_n-sections shown in Fig. 4(c), the plane in Fig. 5(a) is composed of two halves, each with $0 < W_n \leq 1$ and corresponding to either **df**- or **ef**-shear zones. Circular curves in Fig. 5(a) represent special positions where material lines along the apophyses **d** or **e** are not deforming. This occurs at

$$W_n^2 + A_n^2 = 1 \quad \text{(Passchier, 1991; 1997).} \qquad (6)$$

In W_n–A_n–T_n space, equation (6) defines a cylindrical surface parallel to the T_n axis (Fig. 4a).

The circular curves and the $W_n = 1$ and $A_n = T_n = 0$ lines on the $V_n = 0$ plane can be used to classify monoclinic shear zone types (Fig. 5b–d). A subdivision into laterally expansional-, plane strain- or laterally constrictional model shear zones (Fig. 5b) refers to deviations from plane strain flow in the zone. Transpressional-, transtensional-, stretching-, shortening and simple shear model shear zone types (Fig. 1) all plot on just two curves (Fig. 5c–d). Transpressional (TP)- and transtensional (TT) model shear zones (Figs 1 & 5c) develop by non-plane strain flow in the zone (positive or negative stretching rate along the apophysis **f**) but with zero stretching rate along either **d** (**df**-zones) or **e** (**ef**-zones) (e.g. Sanderson and Marchini, 1984). The terms 'thinning' and 'thickening' (Fig. 5c) have a broader significance and refer to all **ef**- or **df**-model shear zones that are instantaneously decreasing or increasing in width (cf. Jones *et al.*, 1997). Stretching (ST)- and shortening (SH) model shear zones (Figs 1 & 5d) develop by plane strain flow in the zone (zero stretching rate along the apophysis **f**) but with positive or negative stretching rate along either **d** or **e** in the shear zone boundary (Coward, 1976; Ramsay, 1980; Kligfield *et al.*, 1981; Sanderson, 1982; Sanderson and Marchini, 1984; Means, 1989; Kligfield and Crespi, 1984; Paterson and Waingler, 1991; Jones *et al.*, 1997). The more general terms 'elongating' and 'contracting' (Fig. 5d) refer to all **ef**- or **df**-model shear zones with positive or negative stretching rate along either **d** (**df**-zones) or **e** (**ef**-zones), without the restriction of plane strain flow. It is obvious from Fig. 5 that even within the restricted group of isochoric **df**- and **ef**-shear zones, the number of possible shear zone types is much greater than the model types presently described in the literature.

Although all model shear zone types in Fig. 5 are geometrically possible, not all types may develop in nature and some may even be dynamically impossible. Unfortunately, very little is known about flow types

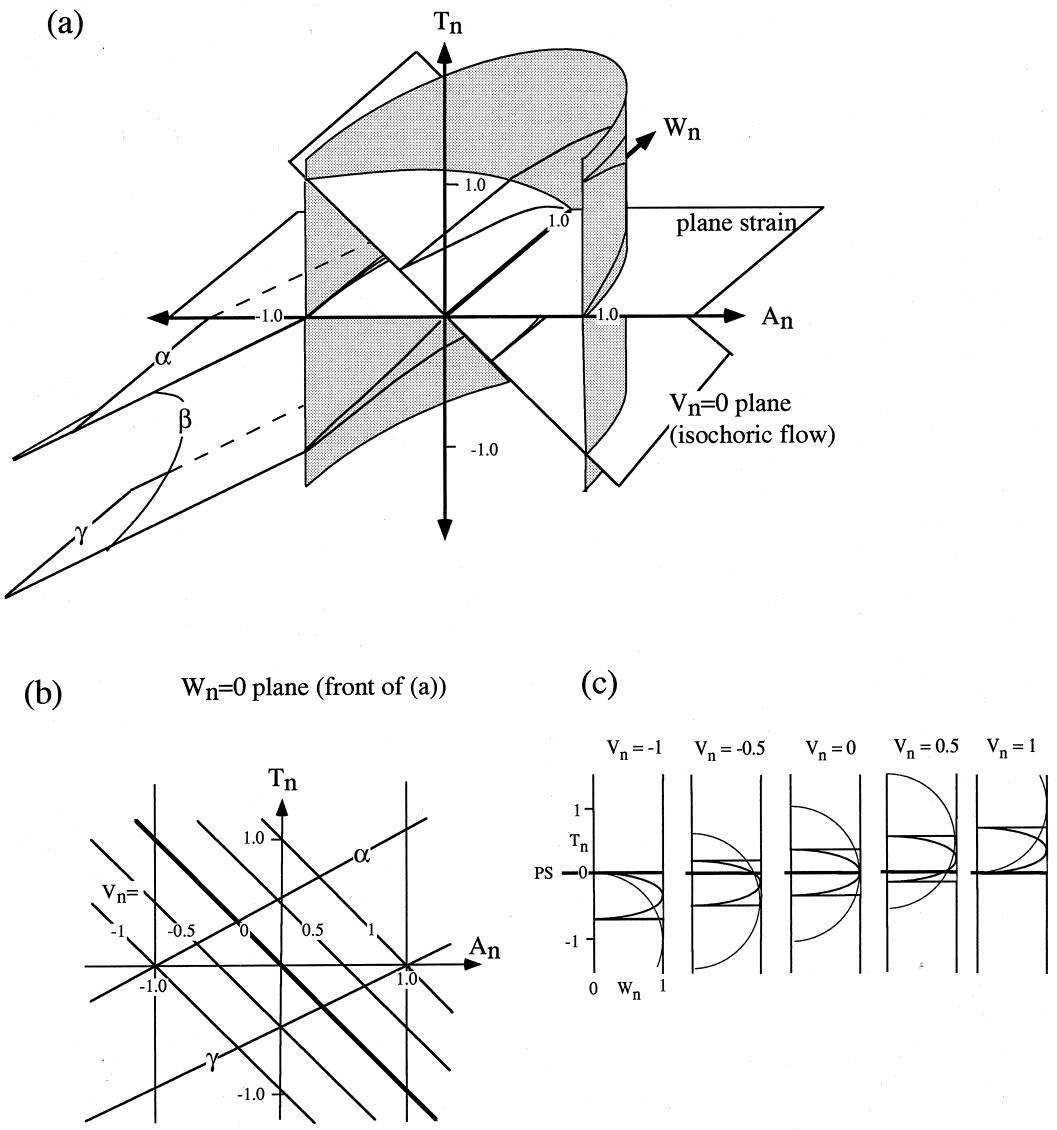

Fig. 4. (a) W_n–A_n–T_n-space in which each monoclinic flow type can be plotted as a point. The ornamented cylindrical surface with vertical axis is the set of all flow types where material lines along one of the apophyses **d** or **e** have zero stretching rate, including transtension and transpression. The horizontal plane is the set of plane-strain flow types. The plane sloping to the right is the set of isochoric flow types (no instantaneous volume change). The left-dipping planes α and γ and cylindrical surface β separate domains where finite strain accumulation by steady-state flow leads to different finite strain classes. Only the lower parts of α, β and γ are shown. (b) Vertical section through (a) normal to the W_n-axis at $W_n = 0$, showing the intersection with planes of flow types with specific V_n-values and with planes α and γ. Two vertical lines at $A_n = -1.0$ and 1.0 mark the intersection with the vertical cylinder in (a). (c) Plane view on the V_n-planes as marked in (b); these planes are oblique cross-sections of the space shown in (a), parallel to the $V_n = 0$ plane. On each plane, the intersection with the $T_n = 0$ plane (plane strain—PS) is indicated by a bold line. Thin horizontal lines are intersections with planes α and γ. The elliptical and circular curves are intersections with surface β and with the vertical cylinder in (a), respectively. Further explanation in text.

and flow history in natural shear zones. Numerical modelling and analogue experiments may help to determine which of the shear zone types presented in Fig. 5 are feasible.

If instantaneous volume change accompanies the development of **df**- and **ef**-shear zones, the zones will plot in other V_n sections of W_n–A_n–T_n space (Fig. 4c) than those of Fig. 5. Figure 6 gives two examples of sections for $V_n = 0.5$ (progressive volume increase) and -0.5 (progressive volume decrease). The fields of shear zone types shown in Fig. 5(a) change in size, simple shear disappears and new shear zone types appear near the centre of the diagram (Fig. 6). The lateral expansional and constrictional fields of Fig. 5(b) shift vertically in Fig. 6, but the boundaries between thinning- and thickening- (Fig. 5c), or between contracting- and elongating-shear zone types (Fig. 5d) do not change.

Summarising, monoclinic model shear zones can be classified according to the orientation of the shear zone boundary with respect to **d** or **e**, and according to the flow type in the zone, either precisely by three

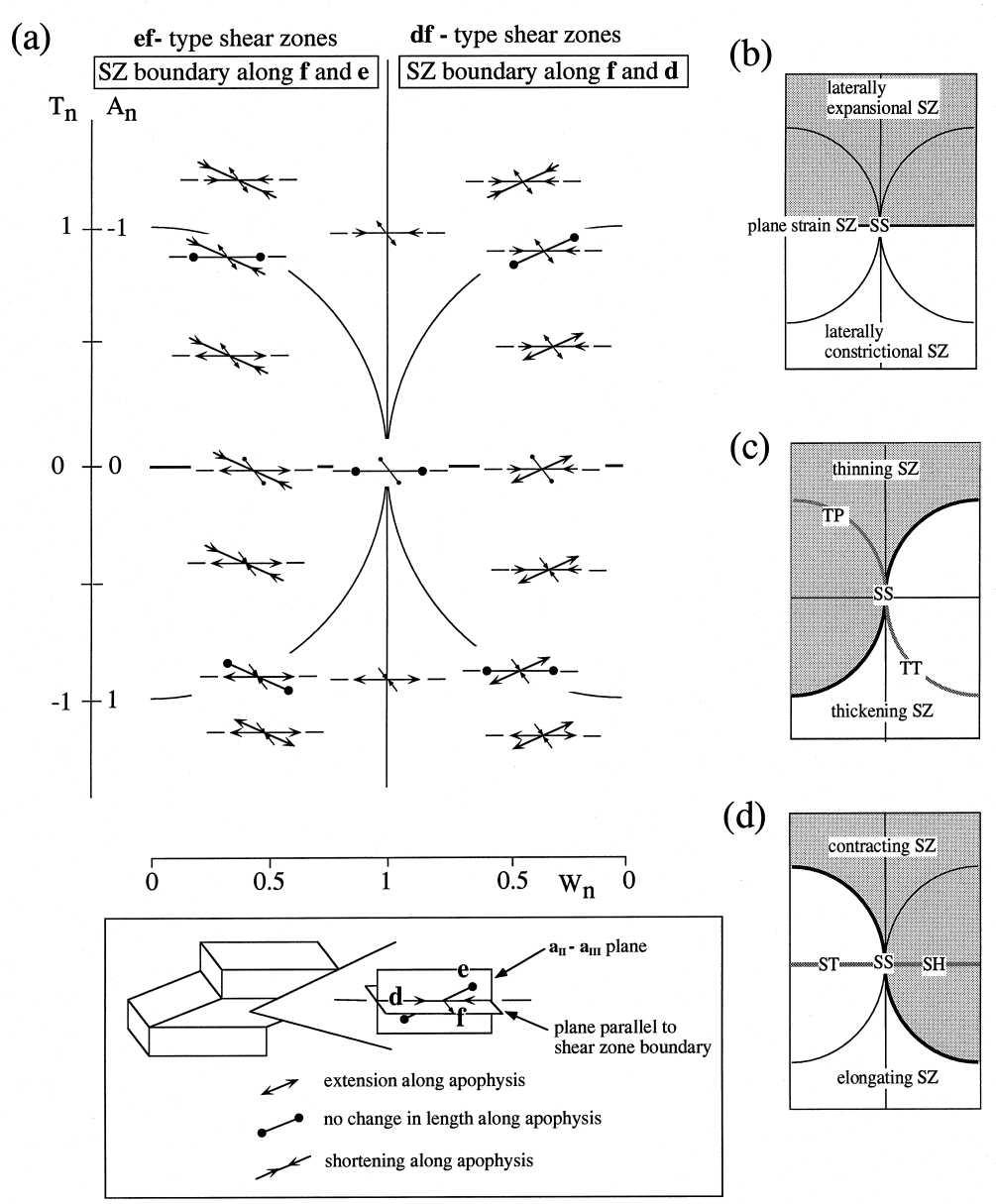

Fig. 5. (a) Diagram showing all possible types of isochoric ($V_n=0$) **df**- and **ef**-shear zones as a function of W_n and T_n or A_n of flow in the zones. W_n is plotted from 1 to 0 in two directions, since either of the apophyses **d** or **e** can be parallel to the shear zone boundary. Schematic illustrations of the stretching behaviour of apophyses in different parts of the diagram are shown. Symbols are explained in the inset. (b–d) Three alternative ways of classifying shear zones using the diagram shown in (a). SZ—shear zone. Shear zone types: SS—simple shear. TP—transpression. TT—transtension. SH—shortening. ST—stretching. Further explanation in text.

normalised numbers (W_n, A_n and T_n) or approximately by classification fields as shown in Fig. 5(b–d).

PROGRESSIVE DEFORMATION IN SHEAR ZONE AND WALL ROCKS

Although classification of model shear zones can be based on flow types, it is also important to know what the effect of such flow types and the orientation of flow axes is on the accumulation of finite strain. In natural shear zones, flow parameters probably change with time during progressive deformation, but little is known about these changes. This section therefore presents simple modelling of progressive deformation in the monoclinic shear zone types shown in Fig. 5 by steady-state flow. The results can serve as reference curves for more complex deformation histories. In the case of constant flow parameters, the geometry of the finite strain ellipsoid is a simple function of flow parameters and time, as outlined below.

For reference purposes, the three possible finite strain axis-orientations in a monoclinic shear zone are labelled $\mathbf{A_I}$, $\mathbf{A_{II}}$ and $\mathbf{A_{III}}$: finite strain axes X, Y and Z lie along these axes. Because of monoclinic flow geometry, $\mathbf{A_I}$ is parallel to the **a_I–f–w** axis of flow (Fig. 2).

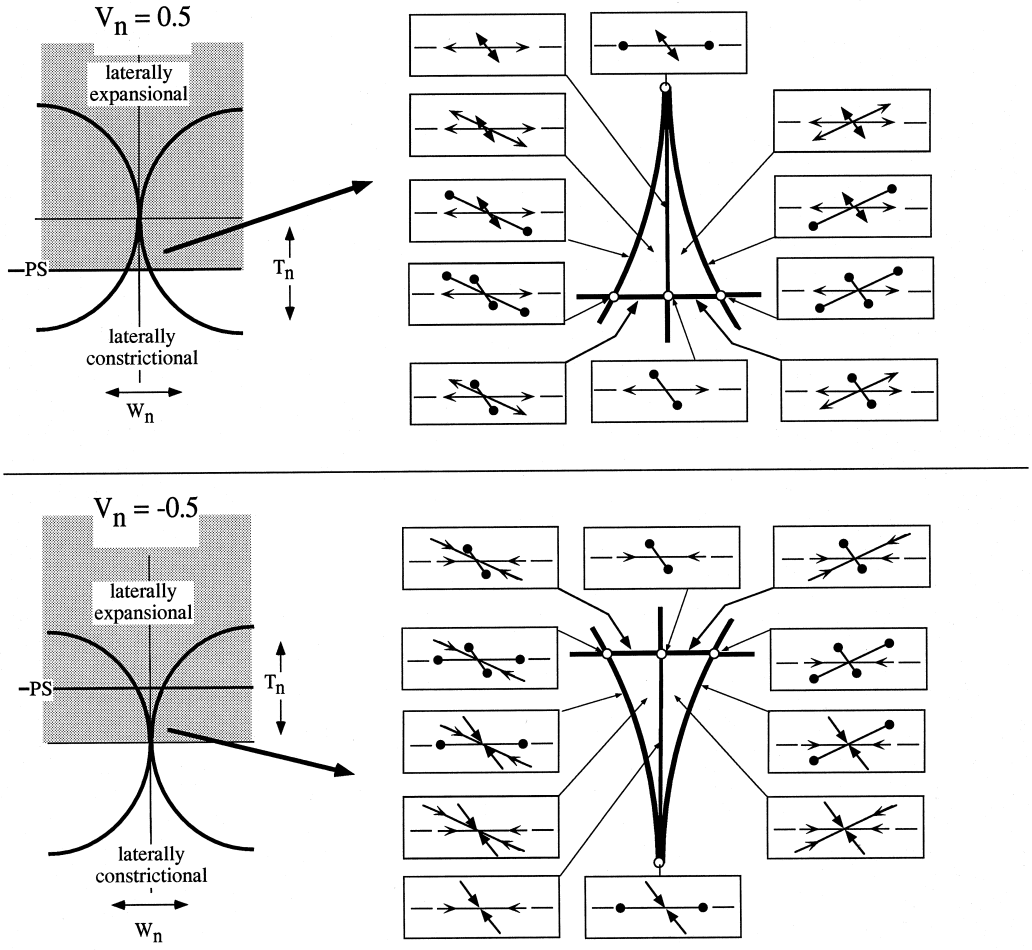

Fig. 6. W_n–T_n diagrams similar to Fig. 5 but for non-isochoric flow conditions ($V_n \neq 0$). Two cross-sections through W_n–A_n–T_n space as shown in Fig. 4(c) are given. Enlargement of the central sector of these diagrams at right shows that a large number of shear zone types appear under these conditions which are not present for isochoric flow in Fig. 5(a). PS—plane strain ($T_n = 0$).

The axial directions $\mathbf{A_{II}}$ and $\mathbf{A_{III}}$ lie in the $\mathbf{a_{II}}$–$\mathbf{a_{III}}$ plane of flow such that $\mathbf{A_{II}}$ lies between the ISA $\mathbf{a_{II}}$ and the apophysis **e**, and $\mathbf{A_{III}}$ normal to $\mathbf{A_I}$ and $\mathbf{A_{II}}$ (Fig. 2). In non-coaxial progressive deformation, $\mathbf{A_{II}}$ and $\mathbf{A_{III}}$ rotate away from the ISA $\mathbf{a_{II}}$ and $\mathbf{a_{III}}$, respectively, in the direction of the apophysis **e** as shown in Fig. 2. For coaxial progressive deformation histories, $\mathbf{A_{II}}$ and $\mathbf{A_{III}}$ remain parallel to $\mathbf{a_{II}}$ and $\mathbf{a_{III}}$. s_I, s_{II} and s_{III} are principal stretch values in directions $\mathbf{A_I}$, $\mathbf{A_{II}}$ and $\mathbf{A_{III}}$ which can be used to calculate strain ratios $R_{II\text{-}I}$ ($= s_{II}/s_I$) and $R_{I\text{-}III}$ ($= s_I/s_{III}$). These ratios can be plotted on a Flinn-diagram in which the orientation of the finite strain ellipsoid can be shown (Fig. 7; Flinn, 1978; Cruden, 1988). Based on the distribution of X, Y and Z over $\mathbf{A_I}$, $\mathbf{A_{II}}$ and $\mathbf{A_{III}}$, the diagram can be subdivided into six main classes of finite strain. Since by definition $a_{II} > a_{III}$ in model shear zones, only three finite strain classes in the upper right part of the diagram can be realised in the shear zones (Fig. 7). These classes have been labelled Z_I, Y_I and X_I after the finite strain axis that lies parallel to direction $\mathbf{A_I}$.

Figure 8(a) illustrates the accumulation of finite strain in model shear zones and their wall rocks as a result of progressive deformation by steady-state flow. Results are shown for **df** or **ef**-model shear zones with isochoric ($V_n = 0$) flow at W_n values of 1.0, 0.7 and 0.0 and T_n values of −0.5, −0.25, 0, 0.25 and 0.5 for each W_n value (Fig. 8a). The calculations were made using equations for strain accumulation presented in Passchier (1997; equations (22)–(27)). For each flow type, a pair of curves is shown in Fig. 8(a), connected by tie-lines which represent time-steps at regular intervals. The solid arrow represents deformation in the model shear zone; the open arrow deformation in a model wall rock.

A coherent interface exists between the shear zone and its wall rock, and the geometry of flow in the model wall rock depends on flow in the shear zone. The paths shown in Fig. 8(a) for progressive deformation in the model wall rock are for isochoric *coaxial* flow with two ISA, $\mathbf{a_I}$ and either $\mathbf{a_{II}}$ (for **ef**-shear zones) or $\mathbf{a_{III}}$ (for **df**-shear zones), parallel to the shear zone boundary. In mechanically realistic shear zones, flow in the wall rock is likely to be non-coaxial with the same shear sense as in the shear zone. The coaxial progressive strain paths for the model wall rock in

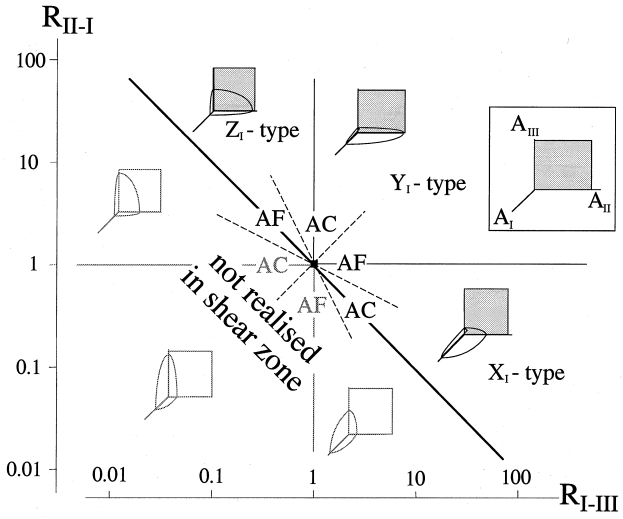

Fig. 7. Modified Flinn-diagram in which the orientation of the finite strain ellipsoid in shear zones can be plotted. Only strain classes to the right of the bold line are realised in model shear zones as defined in this paper; strain states in the wall rock might plot anywhere in the diagram. Finite strain-classes are indicated by a small cartoon showing the orientation of the finite strain ellipsoid with respect to $\mathbf{A_I}$, $\mathbf{A_{II}}$ and $\mathbf{A_{III}}$ (inset). X_I , Y_I and Z_I are specific orientations of the finite strain ellipsoid, named after the principal axis that lies along $\mathbf{A_I}$. Distribution of domains of apparent constriction (AC) and apparent flattening (AF) are indicated in the centre of the diagram.

Fig. 8(a) are meant as reference curves only; strain paths for wall rocks of realistic shear zones may lie somewhere between that of the model wall rock and that of the shear zone.

The following observations can be made from Fig. 8(a):

(1) The length of tie-lines in Fig. 8(a) represents the distance in the Flinn-diagram separating finite strain states in a shear zone and its wall rock. In the case of isochoric progressive deformation as presented in Fig. 8(a), these tie-lines are parallel to the plane-strain ($T_n=0$) curve. At any time during progressive deformation and for any T_n-value, maximum tie-line length is reached for $W_n=1$ in the shear zone and a wall rock that is undergoing coaxial progressive deformation ($W_n=0$); non-coaxial progressive deformation in the wall rock shortens the tie-lines, increasingly so as W_n of flow in the wall rock approaches W_n of flow in the shear zone. Thus, tie-line length at any instant during progressive deformation is dependent on W_n, but independent of T_n of flow in the shear zone.

(2) Differences in finite strain magnitude between a model shear zone and its wall rock depend on W_n and T_n. Finite strain magnitude can be defined as a D_{Flinn}-value in the Flinn-diagram, i.e. as:

$$D_{Flinn}=\sqrt{(\log R_{II-I})^2+(\log R_{I-III})^2} \qquad (7)$$

Curves of equal D_{Flinn}–value are circles centred on the origin of the Flinn-diagram of Figs 7 and 8. Since tie-lines are parallel to the strain path for $T_n=0$ (Fig. 8a), differences in D_{Flinn}–value between a shear zone and its wall rock in the case of isochoric flow are highest for simple shear ($W_n=1$) and plane strain ($T_n=0$).

Natural ductile shear zones are only recognised as such if finite strain (D_{Flinn}) in the shear zone significantly exceeds that in the wall rock. Such a high strain contrast therefore develops most effectively at high W_n and low T_n values of flow in the zone (Fig. 8a).

(3) The difference in two-dimensional finite strain ratio (R_f) between a model shear zone and its wall rock, measured parallel and normal to the displacement direction (Fig. 3), depends on W_n but not on T_n, A_n or V_n. Figure 9 shows two curves, for the $\mathbf{A_{II}A_{III}}$- and $\mathbf{A_IA_{III}}$-sections, respectively, which represent the ratio of R_f between a model shear zone, and a wall rock that deformed by coaxial flow. Both are based on a value of $R_f=100$ in the shear zone. The greatest difference in two-dimensional finite strain between a shear zone and its wall rock develops at high W_n numbers in the shear zone, culminating for simple shear. For example, if we assume that in the $\mathbf{A_{II}A_{III}}$-plane R_f in the shear zone should be at least five times that in the wall rock for a shear zone to be recognisable, W_n should be at least 0.9 (Fig. 9). Since asymmetric structures characteristic of shear zones will also show optimal development at high W_n, very high W_n values between 0.9 and 1 are a prerequisite for well-recognisable *isochoric* monoclinic shear zones. However, in monoclinic model shear zones with volume change, high finite strain ratios between shear zone and wall rock can be reached at lower W_n values, as discussed below.

(4) The symmetry axis for all curves in Fig. 8(a) is the plane strain ($T_n=0$; $\mathbf{R_{II-I}=R_{I-III}}$) line. Strain paths can either stay within one of the three main finite strain categories Z_I, Y_I and X_I (Figs 7 & 8) or pass from one category to another (Fig. 8a; fig. 7 in Passchier, 1997). For such 'cross-over' strain path, there are two possibilities; cross-over from Y_I to Z_I for $T_n<0$, or from Y_I to X_I for $T_n>0$ (Fig. 8a). The exact conditions that lead to development of in-category paths and cross-over paths are derived below.

(5) The longest principal strain axis, X, may be orthogonal in a model shear zone and its wall rock (e.g. for $T_n=0.25$ at $W_n=1$ and $W_n=0.7$ in Fig. 8a). This will occur especially at high W_n, small positive T_n and low finite strain; such shear zones may have stretching- or mineral-lineations *normal* to those in the wall rock. Similarly, the XY-plane may be orthogonal in a model shear zone and its wall rock (e.g. for $T_n=-0.25$ at $W_n=1$ in Fig. 8a). This will occur especially at high W_n, small negative T_n and low finite strain. Such shear zones may have foliations normal to those in the wall rock. If developed in natural shear zones, such conflicting fabric orientations could be erroneously inter-

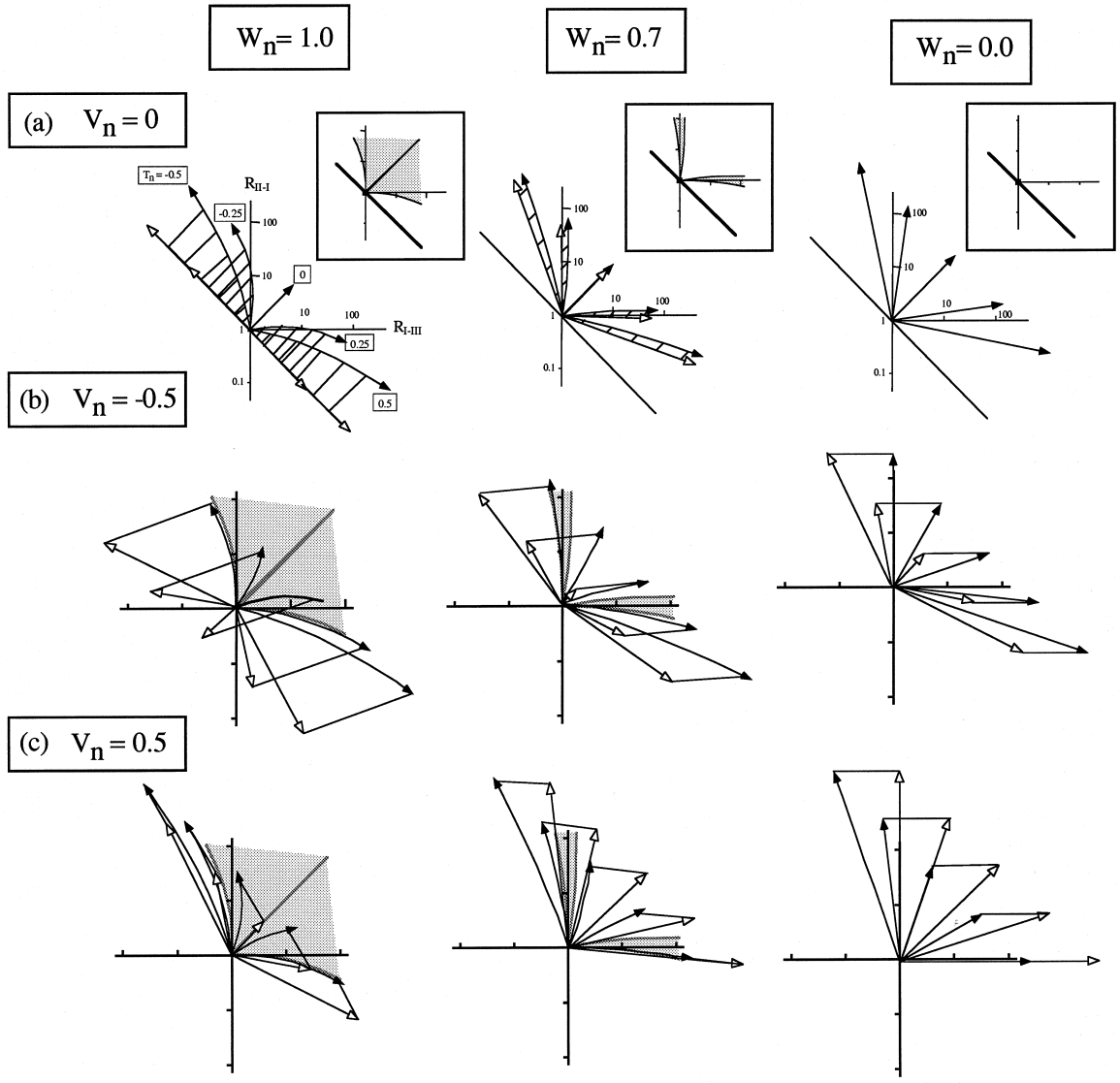

Fig. 8. Finite strain paths plotted in the Flinn-diagram of Fig. 7 for progressive deformation by invariable flow parameters. Diagrams are shown for three different V_n-values, and at each V_n-value for three W_n-values: (a) $V_n = 0$ (isochoric flow); (b) $V_n = -0.5$ (instantaneous volume decrease); (c) $V_n = 0.5$ (instantaneous volume increase). Each diagram shows strain paths for five different T_n values (as indicated by boxes in the top-left diagram). Solid arrows—strain accumulation in a shear zone. Open arrows—strain accumulation in a model wall rock by coaxial progressive deformation, and connected to the shear zone by a coherent boundary. Tie-lines connecting both curves in (a) are spaced at constant strain intervals of $S_t = 5$ (Passchier, 1997) in the shear zone during progressive deformation. In (b) and (c) only tie lines for total strain are shown. Grey fields in the insets of (a) and in (b) and (c) represent domains where strain paths of shear zones can cross over from one finite strain-class of Fig. 7 to another. Shear zone strain paths that lie outside these grey fields will remain within their finite strain class.

preted as unrelated structures belonging to separate phases of deformation.

Strain accumulation with instantaneous volume change

If flow is not isochoric, there are many possible model lines that could be followed such as volume loss in the shear zone only, or volume loss in the shear zone compensated by volume gain in the wall rock. The equations for strain accumulation presented in Passchier (1997; equations (22)–(27)) can also be used to model such progressive deformation with volume change. Figure 8(b & c) gives some examples of progressive deformation with instantaneous volume loss or gain in a shear zone and with isochoric flow in the model wall rock. The main difference with the patterns in Fig. 8(a) is that the diagrams become asymmetric and that significant strain gradients between shear zone and model wall rock are now also possible at lower W_n values.

Boundaries of strain path domains

Strain paths of monoclinic model shear zones accumulated by steady-state flow can remain within one strain category, or pass from one category to another (Fig. 8; Passchier, 1997). The boundaries between categories can be found by investigation of the parent flow

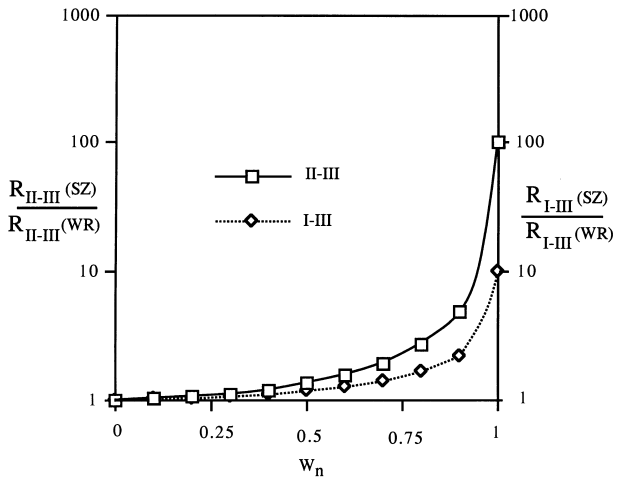

Fig. 9. Diagram showing the effect of W_n on the difference in finite strain ratio (R) between a shear zone and its model wall rock during progressive deformation by steady-state flow. Two R-values are shown in each case: $R_{II\text{-}III}$ and $R_{I\text{-}III}$. Ratios $R_{II\text{-}III}$ and $R_{I\text{-}III}$ in shear zone (SZ) and model wall rock (WR) are plotted against W_n for $R_{II\text{-}III}$ (SZ) = 100. Significant differences in R between a shear zone and its wall rock only occur at high W_n. The result is independent of A_n, T_n and V_n, provided that these are equal in shear zone and wall rock.

types. In the flow geometry chosen here with $a_{II} > a_{III}$, the longest finite strain axis, X, will be either in position $\mathbf{A_I}$, parallel to the apophysis **f** ($\mathbf{f} = \mathbf{a_I}$), or in position $\mathbf{A_{II}}$; this depends on the magnitude of the stretching rates along the ISA $\mathbf{a_I}$, $\mathbf{a_{II}}$ and $\mathbf{a_{III}}$ and the apophysis **e** during progressive deformation.

If $a_I > a_{II}$, X accumulates in $\mathbf{A_I}$-position in all cases. The limiting condition is $a_I = a_{II}$ or in terms of dimensionless numbers using equations (2)–(4);

$$2T_n - A_n = 1 \tag{8a}$$

or using V_n :

$$3T_n - V_n = 1 \quad \text{and} \quad 2V_n - 3A_n = 1 \tag{8b}$$

In the absence of instantaneous volume change when $V_n = 0$, this reduces to:

$$T_n = 1/3 \quad \text{and} \quad A_n = -1/3 \tag{8c}$$

If $a_{II} > a_I$, the situation is more complex and depends on the magnitude of the apophysis **e** and therefore on W_n since:

$$e = \frac{a_{II} + a_{III}}{2} + \frac{a_{II} - a_{III}}{2}\sqrt{1 - W_n^2} \tag{9}$$

This equation can be derived from a Mohr circle construction for flow (Passchier, 1991). If $e > a_I$, material lines in the **f–e** plane will rotate towards the apophysis **e**. In this case, X will lie in position $\mathbf{A_{II}}$ and rotate towards the apophysis **e** for any stage of progressive deformation. The limiting condition is $a_I = e$ or:

$$2T_n - A_n = \sqrt{1 - W_n^2} \tag{10a}$$

or using V_n:

$$3T_n - V_n = \sqrt{1 - W_n^2} \quad \text{and} \quad 2V_n - 3A_n = \sqrt{1 - W_n^2} \tag{10b}$$

or for isochoric flow when $V_n = 0$:

$$T_n = 0.33\sqrt{1 - W_n^2} \quad \text{and} \quad A_n = -0.33\sqrt{1 - W_n^2} \tag{10c}$$

If $a_{II} > a_I > e$, the situation depends on finite strain. The principal finite strain axis X lies in position $\mathbf{A_{II}}$ and rotates towards the apophysis **e** at low finite strain, but with progressive deformation, X can switch from position $\mathbf{A_{II}}$ to $\mathbf{A_I}$ through an intermediate stage of uniaxial flattening. This is a path where the curve of progressive strain accumulation crosses from one strain category to another in Fig. 8. In terms of attractors (Passchier, 1997), either **e** or **f** can be X-attractors under conditions outlined above.

In W_n–A_n–T_n space (Fig. 4a), equations (8) describe a planar surface dipping towards the left (Fig. 4a; plane α). Equations (10) describe an oblique cylindrical surface plunging towards the left (Fig. 4a; surface β). This surface is tangential to plane α at $W_n = 0$ since in that case, equations (10) equal equations (8). In other words, the transitional domain where 'cross-over' of finite strain axes may occur during progressive deformation does not exist for coaxial flow types. Flow at specific rates of instantaneous volume change plot on planes dipping towards the right in Fig. 4(a), and these are shown in Fig. 4(b & c).

In a way similar to that sketched for X, the orientation of the XY plane of the finite strain ellipsoid depends on the magnitude of stretching rates along the ISA $\mathbf{a_I}$, $\mathbf{a_{II}}$ and $\mathbf{a_{III}}$ and the apophysis **d**. Since $a_{II} > a_{III}$, the XY plane can be either the $\mathbf{A_IA_{II}}$- or the $\mathbf{A_{II}A_{III}}$-plane. If $a_{III} > a_I$, the XY plane is the $\mathbf{A_{II}A_{III}}$-plane throughout the deformation history. The limiting condition is $a_I = a_{III}$ or in terms of normalised numbers:

$$A_n - 2T_n = 1 \tag{11a}$$

or using V_n:

$$V_n - 3T_n = 1 \quad \text{and} \quad 3A_n - 2V_n = 1 \tag{11b}$$

In the absence of instantaneous volume change when $V_n = 0$, this reduces to:

$$T_n = -1/3 \quad \text{and} \quad A_n = 1/3 \tag{11c}$$

if $a_I > a_{III}$, the situation is more complex. With progressive deformation, one of the finite strain axes rotates towards the apophysis **e**. If the XY-plane coincides with the $\mathbf{A_{II}A_{III}}$-plane, Z lies along $\mathbf{A_I}$. If the XY-plane is the $\mathbf{A_IA_{II}}$-plane, Z rotates towards **e***, a vector normal to the apophyses **e** and **f**. The stretching rate e^* of a material line instantaneously parallel to **e***

has the same magnitude as the stretching rate d along the apophysis **d** in all monoclinic flow types, as can be deduced from a Mohr circle construction for flow (Passchier, 1991). If $a_I > e^*$, the XY-plane coincides permanently with the $\mathbf{A_IA_{II}}$-plane. If $e^* > a_I > a_{III}$, a switch in orientation of XY from the $\mathbf{A_IA_{II}}$- to the $\mathbf{A_{II}A_{III}}$-plane is possible with progressive deformation. The limiting condition is $a_I = e^*$. Therefore:

$$a_I = e^* = d = \frac{a_{II} + a_{III}}{2} - \frac{a_{II} - a_{III}}{2}\sqrt{1 - W_n^2}. \quad (12)$$

Equation (12) is derived from a Mohr circle construction for flow and can be rewritten as:

$$A_n - 2T_n = \sqrt{1 - W_n^2} \quad (13a)$$

or using V_n:

$$V_n - 3T_n = \sqrt{1 - W_n^2} \quad \text{and} \quad 3A_n - 2V_n = \sqrt{1 - W_n^2} \quad (13b)$$

or for isochoric flow when $V_n = 0$:

$$T_n - 0.33\sqrt{1 - W_n^2} \quad \text{and} \quad A_n = 0.33\sqrt{1 - W_n^2}. \quad (13c)$$

Equations (13) define the same cylindrical surface β in Fig. 4(a) as equations (10); equations (11) define a plane γ in Fig. 4(a). The intersection of planes α and γ and surface β with the $V_n = 0$ and other constant V_n planes are shown in Fig. 4(c). Based on equations (8), (10), (11) and (13), limiting curves can be calculated for progressive deformation histories of shear zones that remain within one finite strain category of Fig. 7, or cross over. These limiting curves are shown in Fig. 8(a) (insets) for isochoric flow. In terms of attractors (Passchier, 1997), either **e*** or **f** can be Z-attractors under conditions outlined above.

If deformation in a model shear zone accumulates by isochoric steady state flow, the dependence of finite strain geometry and orientation on flow parameters can be shown on the plane of isochoric flow types in W_n–A_n–T_n space (Fig. 10a). Boundaries are defined by the intersection of planes α and γ and surface β of Fig. 4(a) with the plane of isochoric flow types. An important difference exists between laterally constrictional and plane strain shear zones on the one hand, and laterally expansional zones on the other (Figs 5b & 10a, b). Transtension (TT), stretching (ST), shortening (SH) and simple shear (SS) shear zones lie in the Z_I and Y_I fields, which implies that X develops in position $\mathbf{A_{II}}$ in the $\mathbf{A_{II}A_{III}}$-plane which also contains the displacement direction (Figs 3 & 10b). Small variations in W_n or A_n will not influence this orientation with the exception of simple shear, where the flow type may move into the field of X_I-class development with a small increase in T_n (Fig. 10a & b). *In fact, simple shear flow is a singularity that is strongly sensitive to small deviations from ideal conditions.*

Transpression (TP) and other laterally expansional shear zone types (Fig. 5b) lie in the X_I- or Y_I-fields, depending on flow conditions (Fig. 10a). In these shear zones, X may develop in either of two orientations; in position $\mathbf{A_{II}}$, or in position $\mathbf{A_I}$ normal to the displacement direction (Figs 10b & 11; Sanderson and Marchini, 1984; Fossen and Tikoff, 1993; Robin and Cruden, 1994; Krantz, 1995).

Similar effects as described above for X exist for the XY plane of finite strain (Figs 10b & 11). Laterally

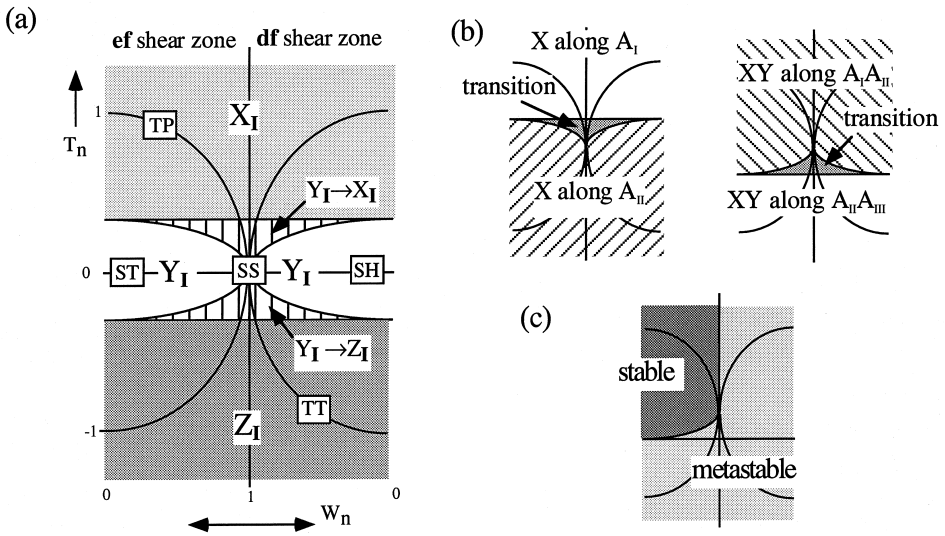

Fig. 10. (a) Diagram as used in Figs 4(c) and 5 in which isochoric flow types in shear zones can be plotted as a function of T_n and W_n. Shading and abbreviations (e.g. X_I, Z_I) refer to the distribution of finite strain classes (Fig. 7) that develop through progressive deformation for steady-state flow in the shear zone. Shear zone types: SS—simple shear. TP—transpression. TT—transtension. SH—shortening. ST—stretching. (b) Subdivision of the T_n–W_n diagram of (a) into fields where X and XY have equal orientation with respect to $\mathbf{A_I}$-, $\mathbf{A_{II}}$- and $\mathbf{A_{III}}$-axes. (c) Stability diagram of shear zone types. All **ef**-shear zone types in the dark domain are stable; those outside the dark domain, and all **df**-shear zone types, are metastable.

expansional shear zone types belong to categories Y_I and X_I, and the XY plane coincides with the $\mathbf{A_I A_{II}}$-plane (Figs 10b & 11). Laterally constrictional shear zones may belong to categories Y_I or Z_I and the XY plane is either the $\mathbf{A_I A_{II}}$-plane, or the $\mathbf{A_{II} A_{III}}$-plane normal to the shear zone boundary.

Strain classes and instantaneous volume change

Figure 4(c) shows the distribution of fields of finite strain categories derived from non-isochoric flow types ($V_n \neq 0$). The obliqueness of the different boundary surfaces in W_n–A_n–T_n space discussed above causes a complex interference in constant V_n sections. With a change in V_n, the boundaries between X_I, Y_I and Z_I domains and the 'transpression–transtension circle' defined by equation (6), 'shift' with respect to the plane strain line (PS in Fig. 4c).

Orientation of finite strain axes in model shear zones

The orientation of finite strain axes in model **df**- and **ef**-shear zones depends on the orientation of the X- or Z-attractors (Passchier, 1997) with respect to shear zone boundaries, and finite strain. The orientation of the attractors depends not only on flow parameters, but also on the nature of the apophyses that are parallel to the shear zone boundary during progressive deformation (Fig. 11). In **ef**-shear zones, the finite strain axis in $\mathbf{A_{II}}$ position rotates towards the shear zone boundary, since the attractor **e** is parallel to the boundary. In **df**-shear zones, however, the attractor **e** is oblique to the shear zone boundary and $\mathbf{A_{II}}$ remains oblique to the boundary, even at high finite strain (Fig. 11).

DISCUSSION

In the previous sections, a purely theoretical treatment was given of all possible types of monoclinic flow, and the types of homogeneous progressive deformation that would accumulate as a result of steady-state flow. Although **df**- and **ef**-monoclinic shear zones are convenient in modelling, there is no reason to believe that natural shear zones must all develop in this way (cf. Jiang and White, 1995; Jiang and Williams, 1998). In natural shear zones with deforming wall rocks flow may be inhomogeneous or, if it is approximately homogeneous in a shear zone segment, it can have a triclinic flow symmetry in which **w** is not parallel to one of the ISA (Jiang and Williams, 1998). One situation where triclinic flow symmetry could be envisaged is where shear zones develop in a pre-existing relatively weak layer or lens bounded by a stronger wall rock, e.g. a gypsum layer bounded by sandstone beds. However, if a new shear zone develops with deforming wall rocks in a homogeneous volume of rock, e.g. a granite mylonite within a granite batholith, its orientation is determined by the local stress field, and principal stress axes are likely to be symmetrically arranged with respect to shear zone boundaries, both in the shear zone and in the wall rock. This will result in monoclinic flow in the shear zone and a monoclinic shear zone symmetry, unless the regional tectonic framework changes orientation during shear zone development. Many shear zones show monoclinic fabric symmetry both in the zone and in relation with fabrics in the wall rock, which suggests that monoclinic flow must be relevant for many ductile shear zones with deforming wall rocks. However, triclinic flow is theoretically possible in ductile shear zones and its relevance in nature should be investigated. Meanwhile, a simple model of steady-state monoclinic flow and progressive deformation can serve as a framework against which natural fabrics can be tested, and can also be used in laboratory and computer modelling of shear zones. In the next sections, some possible consequences of different types of monoclinic flow for natural shear zones are discussed.

X_I-, Y_I- and Z_I-type shear zone segments

Theoretical 'model shear zones' as discussed in this paper with planar, parallel contacts to the wall rock and homogeneous flow in the zone differ from natural shear zones in that these normally have a lateral gradient in flow type from centre to shear zone tips. Model shear zones as treated in this paper, however, can be used to describe the behaviour of small *segments* of natural zones in which flow is approximately homogeneous.

Model shear zone types can be subdivided according to flow parameters (Fig. 5b & c), but also according to finite strain geometry into X_I-, Y_I- and Z_I-type shear zones (Fig. 11). The latter classification is obviously of more practical use for natural shear zones than one based on flow types. Many segments of natural shear zones with a monoclinic fabric geometry can therefore be classified into X_I-, Y_I- or Z_I-type.

Shape fabric geometry need not be identical to finite strain geometry in polyphase natural shear zones (Freeman and Lisle, 1987). For convenience, shape fabric geometry classes are assumed to mimic finite strain geometry classes in the following sections on natural shear zones, i.e. the planar shape fabric element is a foliation parallel to XY and the linear shape fabric element (stretching lineation) is parallel to X.

Unstable shear zone boundaries

The boundaries of model shear zones described in this paper are parallel to flow apophyses **f** and either **d** or **e** and do not rotate with respect to the external reference frame and ISA. It is important, however, to investigate if such shear zone boundary orientations

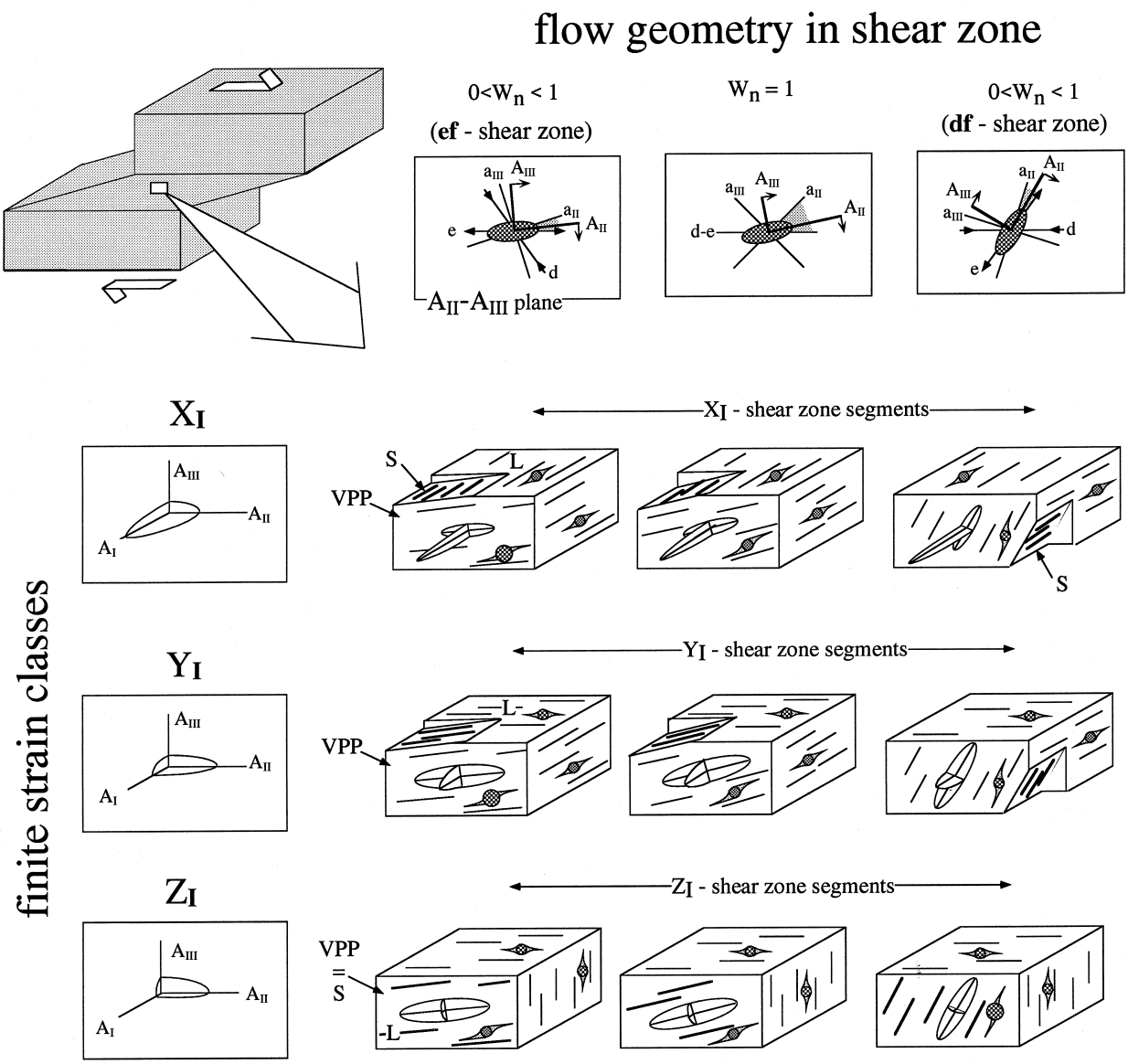

Fig. 11. Diagram showing the effect of the orientation of flow apophyses and of W_n on finite strain geometry and fabric orientation in a developing shear zone segment for the three main finite strain classes or shear zone types X_I, Y_I and Z_I. Each shear zone type is shown by a block diagram in which the shape and orientation of the finite strain ellipsoid and the orientation of planar (S) and linear (L) shape fabric elements are indicated. L is shown as bold lines on S. The front of each block diagram, the $\mathbf{A_{II}A_{III}}$-plane, is the vorticity profile plane (VPP) and shows asymmetric structures, schematically indicated by a mantled porphyroclast; $\mathbf{A_IA_{II}}$- and $\mathbf{A_IA_{III}}$-planes show only symmetric structures. The inclination of the finite strain ellipsoid and of S and L with respect to the model shear zone boundary depends on W_n and on the nature of the apophyses that lie along the shear zone boundary.

are actually stable for small deviations from ideal parallelism with flow apophyses.

Passchier (1997) has shown that flow apophyses can be attractors, transits or repulsors of material lines. However, material planes will only be in a permanently stable position if they are parallel to a pair of apophyses that does not include a repulsor apophysis; in that case, small deviations of the material plane from parallelism with the apophyses will not be amplified, but the plane will tend to return to parallelism. Material planes parallel to an apophysis pair that includes a repulsor will be in metastable position; any small deviation from parallelism will be amplified.

In monoclinic flow types with $a_{II} > a_{III}$, the repulsor-apophysis is **d** if $a_I > d$ and **f** if $d > a_I$, since $a_I = f$ (Passchier, 1987). This implies that the only two stable positions of material planes are the **d–e** (or $\mathbf{A_IA_{II}}$-) plane if $d > a_I$, and the **e–f** plane if $a_I > d$. The limiting condition, $a_I = d$ is given by equation (13). Material planes parallel to the **d–f** plane are therefore never in a stable position, and the same applies to those parallel to the **e–f** plane if $d > a_I$. This applies to shear zone boundaries as well as other material planes such as foliations in a shear zone.

For isochoric flow, only shear zone types plotting in the dark sector of the W_n–T_n-diagram of Fig. 10(c) are

stable monoclinic shear zone types; all other types are in a metastable position. Figure 5 shows that stable types all classify as thinning **ef**-type shear zones, which include transpression-, stretching- and simple shear zones. Thickening shear zones or **df**-type zones are metastable. Simple shear is a special flow type since small deviations of flow parameters towards negative T_n values or to **df**-type shear zones geometry may cause instability (Fig. 10c).

In stable monoclinic shear zone types, small deviations of the boundary from parallelism with the apophyses will not amplify but diminish, and such boundaries are therefore self-stabilising. If the shear zone boundary is in a metastable orientation, any small deviation from exact parallelism will cause the boundary to rotate away from the apophyses. The result could be a mere rotation of a foliation or of shear zone boundaries in the external reference frame, but on a larger scale it could also lead to folding of these structures. Note, however, that in all these cases the symmetry of flow and progressive deformation in the zone remains monoclinic, i.e. the eigenvectors **f** and $\mathbf{a_I}$ remain parallel to **w**.

If flow was steady-state during development of a shear zone, the classification of Fig. 10(a) would apply, and the field of stable shear zones would include X_I and Y_I shear zone types, but no Z_I types.

Inhomogeneous flow in natural shear zones

If flow parameters vary laterally over a ductile shear zone during progressive deformation, gradients can develop from one shear zone type to another. For example, if bulk progressive deformation in a shear zone is of plane strain type ($T_n = 0$), laterally linked variations of T_n may occur in adjacent domains, e.g. if the shear zone is locally thinning and stretching parallel to the apophysis **f**, but thickening and shortening parallel to **f** in adjacent domains (Fig. 12). If this results in a transition from Y_I- to X_I-shear zone segments (Fig. 11), stretching lineations are locally orthogonal to those in the remainder of the zone

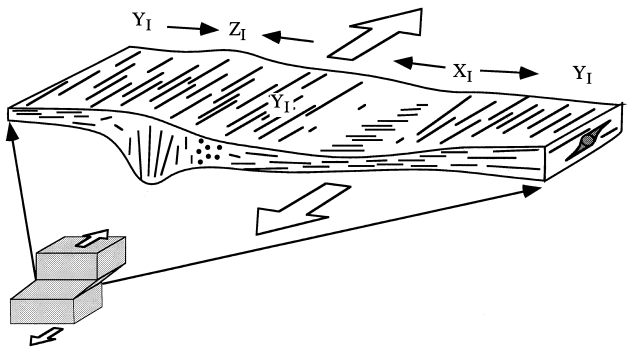

Fig. 12. Cartoon showing the possible lateral variation in shear zone types X_I, Y_I and Z_I in a zone with strong lateral variation in T_n during progressive deformation.

although the vorticity vector has the same orientation throughout (cf. Fossen *et al.*, 1994; Tikoff and Teyssier, 1994; Fig. 12). The transition zone would have no stretching lineation but would be characterised by pure flattening. This structural transition could be mistaken for the effect of two deformation phases. Alternatively, a Y_I-shear zone segment may laterally grade into a Z_I-segment. This may occur through a transition zone with linear fabrics (Fig. 12) or, if the Z_I-shear zone develops in a foliated medium, through a zone of cylindrical folds with axes parallel to the stretching lineation (cf. Passchier *et al.*, in press). Such folds are expected to show increasing tightness towards the Z_I-shear zone segment where they can be isoclinal and even rootless.

Another interesting gradient in flow parameters over a shear zone may occur if one of the wall rocks is stretching more rapidly than the other in the displacement direction. This may lead to a lateral change in W_n, and even a lateral swap in shear sense along a shear zone (cf. Means, 1990). In the shear zone fabric, shear sense swap may occur through a lateral decrease in the asymmetry of fabric elements and a reversal of the geometry of shear sense indicators over a zone with symmetric fabrics. This 'symmetric transition zone' could have foliations and lineations that are similar to those in parts of the zone with asymmetric fabrics. The symmetric transition zone may even shift along the shear zone with time, creating an overprint of two shear senses in some parts of the zone. Such an overprint could be interpreted erroneously as an effect of shear zone reactivation by a second tectonic phase.

Shear sense indicators in monoclinic shear zones

Although precise geometries will have to be determined from modelling studies, a brief outline is given here of how shear sense indicators in general monoclinic shear zones may deviate from those in simple shear zones.

In simple shear zones, asymmetric structures that are commonly used to determine sense of shear such as mantled porphyroclasts, shear band cleavage and mica-fish are best observed on sections normal to the vorticity vector because of their monoclinic overall symmetry. In simple shear zones, this section is parallel to X and normal to the XY-plane or finite strain. In practice, sections are therefore cut parallel to stretching- or mineral-lineations, and normal to the foliation in the shear zone.

In general monoclinic shear zones where flow was not simple shear, asymmetric structures can also be expected to be best developed in a section normal to the vorticity vector (Hanmer and Passchier, 1991). Robin and Cruden (1994) suggested the general term 'vorticity profile plane' (VPP) for such sections and this is the section that has to be found in outcrop to determine displacement direction and sense of shear

(Fig. 11). In the terminology used in this paper, the VPP is always the $\mathbf{A_{II}A_{III}}$-plane of finite strain.

If shape fabric geometry coincides with finite strain geometry, the relation between linear (L) and planar (S) shape fabric elements and the VPP are as follows in X_I-, Y_I- and Z_I-shear zones (Figs 10 & 11);

1. X_I-shear zones: the VPP lies normal to L and S. This is the case for shear zones that form at high T_n values such as some types of transpression
2. Y_I-shear zones: the VPP lies parallel to L and normal to S. This is the case for simple shear, shortening and stretching shear zones.
3. Z_I-shear zones; the VPP lies parallel to L and S. This is the case for shear zones that would form at low T_n values such as some types of transtension.

Shear sense indicators in Y_I-shear zones have been treated in many publications and are familiar to most geologists (Simpson and Schmid, 1983; Hanmer and Passchier, 1991; Simpson and DePaor, 1993). One may speculate what type of shear sense indicators could develop in other shear zone types, and which problems could occur with their recognition.

In the literature, most attention has been paid to the influence of W_n on the geometry of shear sense indicators (Passchier, 1988; Tikoff and Fossen, 1995; Passchier and Trouw, 1995, Chapter 8.3). The main effect is a decrease in the asymmetry of the structure with decreasing W_n (Passchier and Trouw, 1995). Besides W_n, T_n can also be expected to have a strong influence on the three dimensional shape of shear sense indicators, especially in X_I- and Z_I-shear zones; in VPP sections through shear sense indicators in such shear zones, some will show pronounced asymmetry as in Y_I-zones while others show weak or no asymmetry. Figure 13 shows some examples of the problems that may be encountered.

The symmetry of preferred orientation patterns of crystallographic axes are a favoured shear sense indi-

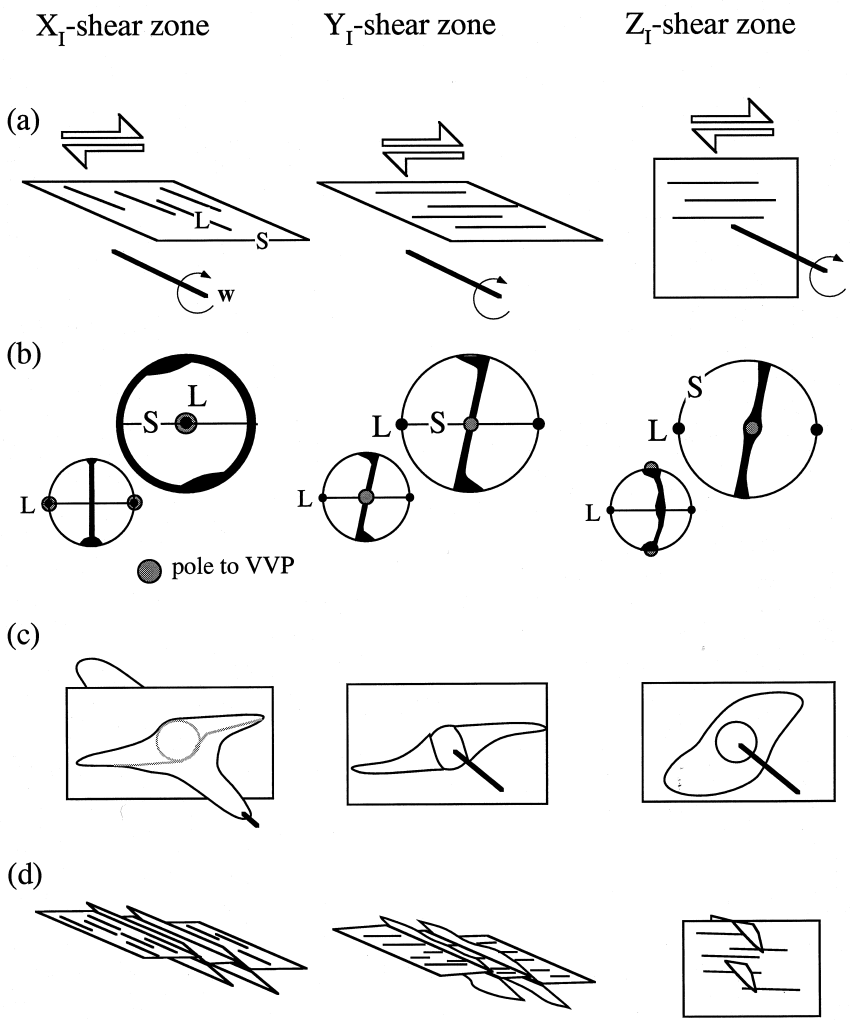

Fig. 13. (a) Orientation of fabric elements in the three main shear zone types. In this example, finite strain geometry equals shape fabric geometry. L—linear shape fabric. S—planar shape fabric. (b) Tentative prediction of low-temperature quartz c-axis preferred orientation patterns that might develop in shear zone types shown in (a). Each pattern is shown in two orientations. (c & d) Tentative prediction of the shape of (c) mantled porphyroclasts and (d) C′-type shear band cleavage transecting the main foliation.

cator. Patterns for Z_I- and X_I-shear zones are likely to be very different from the familiar ones of Y_I-shear zones. The actual patterns are difficult to predict and have to be modelled, but the overall symmetry for quartz *c*-axes and low-T deformation could be as shown in Fig. 13(b). Notice that if these patterns are viewed in the standard reference orientation in a stereogram with vertical foliation S and horizontal lineation L, an unusual asymmetry result that could easily be misinterpreted as being due to polyphase deformation or erroneous sectioning oblique to the desired direction (Fig. 13b).

In Y_I-shear zones, mantled porphyroclasts are important shear sense indicators that develop by recrystallisation in the mantle of a rigid core mineral or mineral aggregate, and ductile deformation of the mantle around the rigid core to an asymmetric shape (Passchier and Trouw, 1995). In X_I-shear zones, the mantle will be elongated in the $\mathbf{A_I}$-direction (Figs 2 & 13c), but in VPP ($\mathbf{A_{II}A_{III}}$) sections a similar asymmetry as in Y_I-shear zones, albeit with shorter wings, can be expected. In Z_I-shear zones, however, the wings will lie almost completely in the foliation ($\mathbf{A_{II}A_{III}}$) plane, and the asymmetry is probably weak or even absent (Fig. 13c).

C′-type shear band cleavage develops in many Y_I-shear zones that have a strong foliation, probably by flow partitioning in response to the strong planar anisotropy (Passchier and Trouw, 1995). The geometry will be as shown in Fig. 13(d), centre. In X_I-shear zones, shear bands can be expected to show a more planar geometry because of the extension parallel to $\mathbf{A_I}$, but since foliations will tend to develop in the $\mathbf{A_IA_{II}}$-plane, shear band cleavage can be expected to develop. In the VPP, shear bands in X_I-shear zones will therefore have a similar geometry to that in Y_I-shear zones. In Z_I-shear zones, however, the foliation tends to develop normal to $\mathbf{A_I}$ and to the vorticity vector; in this orientation, it seems unlikely that strong shear bands can develop. The most spectacular C′-type shear band cleavage in shear zones has been reported from shear zones in an extensional tectonic setting (Passchier, 1991), and it is quite conceivable that such zones are in fact elongating shear zones (Fig. 5d).

Analysis of natural monoclinic shear zones

If a volume of mylonite with a straight planar and linear shape fabric has shear sense indicators with a symmetry axis normal or parallel to elements of this fabric, they may have developed by monoclinic flow. In that case, they could be analysed as follows. First, rock faces are identified on which fabric elements with monoclinic symmetry, such as shear sense indicators, are best developed. These rock faces will be close to the orientation of the VPP, and the symmetry axis is normal to this plane. From the orientation of the VPP with respect to X and XY in the shear zone fabric, the zone or zone segment can be classified as X_I-, Y_I- or Z_I-type.

Natural high-strain planar ductile shear zones reported in the literature are mostly Y_I-zones, but X_I-zones, with the XY-plane at a small angle to the shear zone boundary have been reported, amongst others, from the Canadian shield (Hudleston *et al.*, 1988; Robert, 1989; Robin and Cruden, 1994), the Canadian Cordillera (McDonough and Simony, 1989), Sweden (Talbot and Sokoutis, 1995), the Kola peninsula (Alekseev *et al.*, 1996), NE-Spain (Carreras and Druguet, 1994; Druguet *et al.*, 1997) and the Sierra Nevada Batholith, California (Tikoff and Greene, 1997). Y_I- and X_I-shear zones correspond exactly to the model **ef**-shear zone geometries that would form from flow types that plot in the *stable* sector of Fig. 10(c). Z_I-shear zones (Fig. 11), which can theoretically be formed by compression along the vorticity vector (Fig. 7) have apparently not been recorded as natural shear zones, except for a possible case in west Greenland (Passchier *et al.*, in press). This may be due to the fact that Z_I-shear zones plot in the metastable field of Fig. 10(c). Z_I-zones may not develop as high-strain planar shear zones, but only as minor domains within shear zones of another type, e.g. associated with intense folding of foliations parallel to the lineation. If Z_I-shear zone types exist in nature they will also be difficult to recognise in the field; foliations develop normal to the vorticity vector, and shear sense indicators are therefore expected to be weakly developed.

Stretching and mineral lineations and shear sense indicators in ductile shear zones are important tools to determine relative movement direction of wall rocks (Simpson and Schmid, 1983; Hanmer and Passchier, 1991) and large-scale tectonic transport directions (e.g. Shackleton and Ries, 1984). It is therefore important to correctly classify monoclinic shear zone types into one of the categories mentioned above. If Z_I- or X_I-shear zones are mistaken for Y_I-shear zones, rock-sections other than the $\mathbf{A_{II}A_{III}}$-plane will be assumed to represent the VPP. As a result, the displacement direction of the shear zone can be erroneously interpreted to lie orthogonal to the true direction. Another problem is that the monoclinic symmetry axis of the fabric may be contained within the plane of section (Fig. 11). Consequently, the fabrics that are found will be all symmetric, and the shear zone may be dismissed as 'a useless one' without clear shear sense indicators, or it may locally give conflicting information.

The angle between X or the XY-plane in a shear zone and the shear zone boundary may be used to distinguish natural **ef**- or **df**-monoclinic shear zones. In **ef**-shear zones, the fabric in the highest-strain domains of the zone approaches parallelism with the shear zone boundary; simple shear is a well-known example (Fig. 11). However, if **df**-shear zones exist in nature, the fabric in the highest-strain domains will approach

a steep orientation, oblique to the shear zone boundary and corresponding to the orientation of the attractor in the $\mathbf{A_{II}A_{III}}$-plane (Fig. 11).

CONCLUSIONS

1. Flow geometry in monoclinic model shear zones can be completely described by three kinematic numbers W_n, T_n and A_n. The published model shear zone geometries such as simple shear-, transpression-, transtension-, shortening- and stretching shear zones are only a few of a range of possible types.
2. Progressive deformation by steady-state monoclinic flow can produce three types of shear zones, classified by finite strain geometry and orientation; X_I-, Y_I- and Z_I-type. Y_I shear zones, the standard type, have the strain geometry of simple shear zones; X_I zones have X parallel to the vorticity vector, and Z_I zones have XY normal to the shear zone boundary. In some cases a switch from Y_I- to X_I- or Z_I-shear zone type is possible with progressive deformation. Confusion of Z_I or X_I zones for standard Y_I shear zones may cause errors in the reconstruction of sense of shear and direction of tectonic transport.
3. Gradients in flow parameters within a shear zone may cause lateral gradients in shear zone type (Y_I, X_I or Z_I).
4. Only a small part of the geometrically possible monoclinic model shear zone types are expected to be stable, including some Y_I- and X_I- but no Z_I-types. Natural shear zone types described in the literature fit within the predicted domain of stable monoclinic shear zones, which suggests that natural metastable shear zone types may not exist, or do not develop into easily recognisable high-strain planar shear zones.

Acknowledgements—This study was partly financed by the Volkswagen Stiftung. The paper benefited from reviews by B. Tikoff, D. Oertel, P. Robin and discussion with W. Means, C. Talbot, A. Cruden and D. Sokoutis.

REFERENCES

Alekseev, V., Unzog, W. and Wallbrecher, E. (1996) A field example of *b*-lineation. *Erweiterte Kurzfassungen zum 6. Symposium Tektonik–Strukturgeologie–Kristallingeologie, Salzburg*. 10–15 April 1996, pp. 1–4.

Carreras, J. and Druguet, E. (1994) Structural zonation as a result of inhomogeneous non-coaxial deformation and its control on syntectonic intrusions: an example from the Cap de Creus area, eastern Pyrenees. *Journal of Structural Geology* **16,** 1525–1534.

Coward, M. P. (1976) Strain within ductile shear zones. *Tectonophysics* **34,** 181–197.

Cruden, A. R. (1988) Deformation around a rising diapir modelled by creeping flow past a sphere. *Tectonics* **7,** 1091–1101.

Druguet, E., Passchier, C. W., Carreras, J., Victor, P. and den Brok, S. (1997) Analysis of a complex high-strain zone at Cap de Creus, Spain. *Tectonophysics* **280,** 31–45.

Flinn, D. (1978) Construction and computation of three-dimensional progressive deformations. *Journal of the Geological Society of London* **135,** 291–305.

Fossen, H. and Tikoff, B. (1993) The deformation matrix for simultaneous simple shearing, pure shearing and volume change, and its application to transpression–transtension tectonics. *Journal of Structural Geology* **15,** 413–422.

Fossen, H., Tikoff, B. and Teyssier, C. (1994) Strain modeling of transpressional and transtensional deformation. *Norsk Geologisk Tidsskrift* **74,** 134–145.

Freeman, B. and Lisle, R. J. (1987) The relationship between tectonic strain and the three-dimensional shape fabric of pebbles in deformed conglomerates. *Journal of the Geological Society London* **144,** 635–639.

Hanmer, S. and Passchier, C. W. (1991) Shear sense indicators: a review. *Geological Survey of Canada*. Paper 90.

Harland, W. B. (1971) Tectonic transpression in Caledonian Spitzbergen. *Geological Magazine* **108,** 27–42.

Hudleston, P. J., Schultz-Ela, D. and Southwick, D. L. (1988) Transpression in an Archean greenstone belt, northern Minnesota. *Canadian Journal of Earth Sciences* **25,** 1060–1068.

Ingles, J. (1983) Theoretical strain patterns in ductile zones simultaneously undergoing simple shear and bulk shortening. *Journal of Structural Geology* **5,** 369–382.

Jiang, D. and White, J. C. (1995) Kinematics of rock flow and the interpretation of geological structures, with particular reference to shear zones. *Journal of Structural Geology* **17,** 1249–1265.

Jiang, D. and Williams, P. F. (1998) High-strain zones: a unified model. *Journal of Structural Geology* **20,** 1105–1120.

Jones, R. R. and Tanner, P. W. G. (1995) Strain partitioning in transpression zones. *Journal of Structural Geology* **17,** 793–802.

Jones, R. R., Holdsworth, R. E. and Bailey, W. (1997) Lateral extrusion in transpression zones: the importance of boundary conditions. *Journal of Structural Geology* **19,** 1201–1217.

Kligfield, R. and Crespi, J. (1984) Displacement and strain patterns of extensional orogens. *Tectonics* **3,** 577–609.

Kligfield, R., Carmignani, L. and Owens, W. H. (1981) Strain analysis of a northern Apennine shear zone using deformed marble breccias. *Journal of Structural Geology* **3,** 421–436.

Krantz, R. W. (1995) The transpressional strain model applied to strike-slip, oblique-convergent and oblique-divergent deformation. *Journal of Structural Geology* **17,** 1125–1137.

Lister, G. S. and Williams, P. F. (1983) The partitioning of deformation in flowing rock masses. *Tectonophysics* **92,** 1–33.

McDonough, M. R. and Simony, P. S. (1989) Valemount strain zone: A dextral oblique-slip thrust system linking the Rocky Mountain and Omineca belts of the south-eastern Canadian Cordillera. *Geology* **17,** 237–240.

Means, W. D. (1989) Stretching faults. *Geology* **17,** 893–896.

Means, W. D. (1990) One-dimensional kinematics of stretching faults. *Journal of Structural Geology* **12,** 267–272.

Passchier, C. W. (1987) Stable positions of rigid objects in non-coaxial flow—a study in vorticity analysis. *Journal of Structural Geology* **9,** 679–690.

Passchier, C. W. (1988) Analysis of deformation paths in shear zones. *Geologische Rundschau* **77,** 309–318.

Passchier, C. W. (1991) The classification of dilatant flow types. *Journal of Structural Geology* **13,** 101–104.

Passchier, C. W. (1997) The fabric attractor. *Journal of Structural Geology* **19,** 113–127.

Passchier, C. W. and Trouw, R. A. J. (1995) *Microtectonics*. Springer-Verlag, Heidelberg.

Passchier, C. W., den Brok, S. W. J., van Gool, J. A. M., Marker, M. and Manatschal, G. (1997) A laterally constricted shear zone system—the Nordre Strømfjord steep belt, Nagssugtoqidian Orogen, W. Greenland. *Terra Nova* **9,** 199–202.

Paterson, S. R. and Wainger, L. (1991) Strains and structures associated with a terrane bounding stretching fault: the Melones fault zone, central Sierra Nevada, California. *Tectonophysics* **194,** 69–90.

Ramberg, H. (1975) Particle paths, displacement and progressive strain applicable to rocks. *Tectonophysics* **28,** 1–37.

Ramsay, J. G. (1980) Shear zone geometry: a review. *Journal of Structural Geology* **2,** 83–101.

Ramsay, J. G. and Huber, M. I. (1983) *The Techniques of Modern Structural Geology. Vol 1—Strain Analysis*. Academic Press, London.

Robert, F. (1989) Internal structure of the Cadillac tectonic zone southeast of Val d'Or, Abitibi greenstone belt, Quebec. *Canadian Journal of Earth Sciences* **26,** 2661–2675.

Robin, P. Y. F. and Cruden, A. R. (1994) Strain and vorticity patterns in ideally ductile transpression zones. *Journal of Structural Geology* **16,** 447–466.

Sanderson, D. J. (1982) Models of strain variation in nappes and thrust sheets: a review. In *Strain within Thrust Belts*. ed. G. D. Williams. *Tectonophysics* **88,** 201–233.

Sanderson, D. J. and Marchini, R. D. (1984) Transpression. *Journal of Structural Geology* **6,** 449–549.

Shackleton, R. M. and Ries, A. C. (1984) The relation between regionally consistent stretching lineations and plate motions. *Journal of Structural Geology* **6,** 111–120.

Simpson, C. and DePaor, D. G. (1993) Strain and kinematic analysis in general shear zones. *Journal of Structural Geology* **15,** 1–20.

Simpson, C. and Schmid, S. M. (1983) An evaluation of criteria to determine the sense of movement in sheared rocks. *Geological Society America Bulletin* **94,** 1281–1288.

Talbot, C. J. and Sokoutis, D. (1995) Strain ellipsoids from incompetent dykes: application to volume loss during mylonitization in the Singögneiss zone, central Sweden. *Journal of Structural Geology* **17,** 927–948.

Tikoff, B. and Fossen, H. (1993) Simultaneous pure and simple shear—the unifying deformation matrix. *Tectonophysics* **217,** 267–283.

Tikoff, B. and Teyssier, C. (1994) Strain and fabric analyses based on porphyroclast interaction. *Journal of Structural Geology* **16,** 477–492.

Tikoff, B. and Fossen, H. (1995) The limitations of three-dimensional kinematic vorticity analysis. *Journal of Structural Geology* **17,** 1771–1784.

Tikoff, B. and Greene, D. (1997) Stretching lineations in transpressional shear zones: an example from the Sierra Nevada Batholith, California. *Journal of Structural Geology* **19,** 29–41.

Weijermars, R. (1991) The role of stress in ductile deformation. *Journal of Structural Geology* **13,** 1061–1078.